POLITECNICO DI TORINO
Repository ISTITUZIONALE

Natural Zeolites for Sustainable Ammonium Removal in Decentralised Wastewater Treatment: An Experimental Study

*Original*
Natural Zeolites for Sustainable Ammonium Removal in Decentralised Wastewater Treatment: An Experimental Study / Ravina, M., Marotta, E., Zanetti, M.. - In: SUSTAINABILITY. - ISSN 2071-1050. - 18:13(2026). [10.3390/su18136396]

*Availability:*
This version is available at: 11583/3016788 since: 2026-10-19T12:28:46Z

*Publisher:*
MDPI

*Published*
DOI:10.3390/su18136396

*Terms of use:*

This article is made available under terms and conditions as specified in the corresponding bibliographic description in the repository

*Publisher copyright*

(Article begins on next page)

15 November 2026

*sustainability*

MDPI

*Article*

# Natural Zeolites for Sustainable Ammonium Removal in Decentralised Wastewater Treatment: An Experimental Study

**Marco Ravina *, Edoardo Marotta and Mariachiara Zanetti**

Department of Environment, Land and Infrastructure Engineering, Politecnico di Torino, Corso Duca degli Abruzzi 24, 10129 Torino, Italy

* Correspondence: marco.ravina@polito.it

**Abstract**

Sustainable and efficient removal of nutrients in decentralised wastewater treatment is still challenging. This work focused on the characterisation of natural clinoptilolite and chabasite as low-cost and recyclable ammonium adsorbents. Inductively coupled plasma analysis showed Si/Al ratios of 3.92 and 2.30 for clinoptilolite and chabasite, respectively. X-ray diffraction tests showed different material purities (93% for clinoptilolite and 73% for chabasite). The Brunauer–Emmett–Teller (BET) reported specific areas of 291.6 $m^2 \cdot g^{-1}$ and 29.9 $m^2 \cdot g^{-1}$ for chabasite and clinoptilolite, respectively. Single point pore volume at $P/P_0 = 0.99$ was 0.2 $cm^3\ g^{-1}$ and 0.12 $cm^3\ g^{-1}$ for chabasite and clinoptilolite, respectively. Adsorption capacities derived from batch adsorption tests were $1.66 \pm 0.08$ $mg \cdot g^{-1}$ and $1.47 \pm 0.03$ $mg \cdot g^{-1}$ for clinoptilolite and chabasite, respectively ($C_{eq} = 10$ $mg \cdot L^{-1}$). In all column tests, the adsorption capacity of clinoptilolite was higher ($2.48 \pm 0.3$ vs. $2.21 \pm 0.2$ $mg \cdot g^{-1}$), a result inconsistent with its lower exchange capacity and lower specific surface area. Although it is difficult to clearly define the leading mechanism for adsorption, the difference between the two materials is probably due to the slower adsorption kinetics of chabazite, while the purity of the material may also have contributed. Applications of these sustainable materials for ammonium adsorption in decentralised wastewater treatment is promising, although determining their detailed preliminary characterisation is fundamental.

**Keywords:** decentralised wastewater treatment; sustainable adsorbents; natural zeolites; nutrient removal; clinoptilolite; chabasite

Check for updates

Academic Editors: Viktor Koval, Jairo González-Bueno and Rima Tamošiūnienė

Received: 5 May 2026
Revised: 17 June 2026
Accepted: 22 June 2026
Published: 23 June 2026

**Copyright:** © 2026 by the authors. Licensee MDPI, Basel, Switzerland. This article is an open access article distributed under the terms and conditions of the Creative Commons Attribution (CC BY) license.

## 1. Introduction

Water treatment, particularly in developing countries, requires decentralised plants that guarantee adequate pollutant removal efficiency at limited costs. These plants usually make use of low-cost or nature-based solutions, which sometimes have limitations in the removal efficiency of certain components, such as nutrients [1]. When the effluent to be treated comes from septic tanks or pit latrines, nitrogen is present in high concentrations, especially in the ammoniacal (reduced) form. In the last several decades, experimental studies for ammonia nitrogen removal from water have steadily advanced. Ammonium compounds are characterised by an extreme solubility in the presence of water. Ammonium nitrogen in water can have negative impacts on aquatic ecosystems, leading to toxicity in fish and other organisms, disrupting the natural balance through eutrophication, and potentially impacting human health if consumed [2]. Removing ammonium requires complex treatments: biological treatments (nitrification and denitrification, biodegradation),

chemical treatments (oxidation, chlorination), electrochemical and chemical–physical treatments (ionic exchange) [3,4]. Breakpoint chlorination is the most widely used method for ammonia removal. Despite its effectiveness, though, this method of treating water leads to the creation of organohalogen chemicals that have been linked to cancer [2]. Biological treatments are often the most effective method for nutrient removal in wastewater, but their complexity can make them difficult to implement in certain contexts [5]. Emerging insights into biological nitrogen transformation have only been described recently [6]. Biological processes necessitate considerable operational and maintenance expenditures, as well as careful control of operating parameters such as pH, dissolved oxygen, and temperature [7]. In anaerobic membrane bioreactors, pH regulation and fouling mitigation are still major challenges [8]. Additionally, tank aeration is associated with a significant demand for energy [9]. Advanced oxidation processes have been extensively studied with high resulting performance but high energy consumption [10]. Since neither chemical nor biological processes are easily applicable in these processes, the removal efficiency of ammonium can be limited [11], thus constricting the water reuse possibilities.

Adsorption can be a viable alternative for wastewater purification [12,13]. The crucial challenge in the adsorption process is to select an appropriate adsorbent with optimal characteristics, including high adsorption capacity, selectivity, rapid adsorption kinetics, and reusability [14]. Synthetic materials offer tunability but at a higher cost [15]. In order to keep costs reasonable, the adsorbent material must demonstrate high adsorption capacity and be economical, easy to handle, and readily available [16].

Natural zeolites are abundant materials on Earth, potentially suitable for this purpose. Zeolites are crystalline minerals with a structure formed by interconnected tetrahedra. In zeolites, the replacement of Si for Al results in a negative charge in the lattice, which is typically counterbalanced by additional framework cations, also known as exchangeable cations (Na, K, Ca, etc.), which can be readily replaced by other cations. The zeolite mineral that forms is controlled mostly by the pH of the water solutions involved and the Si/Al ratio in the initial material [17]. Zeolites created from volcanic rocks that are rich in silica are mostly clinoptilolite–mordenite-rich. Comparatively silica-poor rocks, however, mostly form zeolites that are rich in phillipsite and chabasite [4]. Zeolites are not limited to natural minerals, but are often prepared synthetically for industrial processes requiring fine-tuned materials. Their structure comprises cavities and channels that are occupied by water molecules or extra-lattice cations, which are capable of exchanging cations when in contact with an electrolyte solution [18].

Ion exchange is the process of exchanging ions between a liquid and a solid phase. The solid phase is charged and this charge is balanced by ions of the opposite charge, named counterions. Cation exchange capacity (CEC) is defined as the amount of positive charge that can be exchanged per mass of solid. Zeolites are widely used in ion exchange applications, where they exchange cations from their structure with dissolved ones [16].

Zeolites have been widely studied over the past decades for contaminant adsorption from wastewater, in both natural and chemically or physically modified forms [19]. Nevertheless, the adsorption behaviour of zeolites still needs to be fully understood through detailed characterisation studies [20]. A key parameter for the adsorption behaviour of zeolites is the silicon-to-aluminium ratio (Si/Al). The Si/Al ratio can vary from 1 to 46 [21].

Other primary characteristics of zeolites are their porosity, cation exchange capacity, and reversible dehydration. The channels permit a high degree of selectivity due to the crystalline structure, which defines regular cells capable of capturing both liquid and gaseous molecules for adsorption. This capacity generally rises with increasing pressure and decreasing temperature, although this behaviour may not apply in more complex systems, such as in chemisorption processes or when specific interactions occur between the

adsorbent and the adsorbate. Zeolites exhibit a preference (selectivity) for specific cations. Clinoptilolite and chabasite have been shown to have a strong affinity with ammonium [22].

Clinoptilolite is a natural zeolite whose composition can vary slightly depending on the origin of the mineral. The generic formula of clinoptilolite is $M_{3–6}(Al_6Si_{30})O_{72}{\cdot}20(H_2O)$, where M represents exchangeable cations, mainly sodium ($Na^+$), potassium ($K^+$) and calcium ($Ca^{2+}$). The number of these cations varies to balance the charge of the structure [23]. Al, Si, O represent the skeleton of the zeolite, made up of silicon tetrahedra ($SiO_4$) and aluminium ($AlO_4$) linked together. Its composition can vary depending on its origin [24]. Also, the Si/Al ratio may vary slightly and has an impact on the properties of zeolite [25]. Chabasite is also a natural zeolite whose composition can be variable. The generic formula for chabasite is $M(Al_2Si_4O_{12}){\cdot}6H_2O$, where M represents one or more metal cations (usually divalent such as $Ca^{2+}$, or monovalent such as $Na^+$ and $K^+$) [26,27].

In the present study, two types of natural unmodified zeolites (clinoptilolite and chabasite) were characterised and tested by means of a series of experimental measurements under both static and dynamic conditions. The objective was to characterise the adsorption capacity of these materials against water-dissolved ammonium ions ($NH_4^+$), in order to assess their possible application in water treatment plants. Experimental tests were run at low initial ammonium concentration (10 $mg{\cdot}L^{-1}$), in order to evaluate the potential use of these adsorbent materials in low-cost filtration systems, which could also be applied in decentralised treatment plants. The research design proposed in this study aims to address aspects that remain insufficiently characterised in the existing literature. While a large proportion of previous studies have focused on engineered adsorbents and treatment systems designed to remove ammonium from highly concentrated solutions (typically in the order of hundreds of mg $L^{-1}$), practical applications in decentralised wastewater treatment often involve considerably lower residual ammonium concentrations. The novelty of the present work lies in the direct comparison of two commercially available natural zeolites, clinoptilolite and chabasite, under a consistent experimental framework combining detailed material characterisation, equilibrium batch adsorption tests, and long-term fixed-bed column experiments. Particular attention was devoted to low initial ammonium concentrations (10 mg $L^{-1}$), representative of partially treated wastewaters requiring tertiary polishing treatments. In addition, adsorption columns were characterised through tracer tests, allowing the estimation of transport parameters such as the retardation factor and hydrodynamic dispersion coefficient. These parameters, together with the experimentally determined adsorption capacities and breakthrough curves, provide information directly relevant to the design of real low-cost filtration systems, including adsorbent sizing, expected service life, and prediction of breakthrough behaviour under operating conditions.

## 2. Materials and Methods

### *2.1. Zeolites Employed*

Two types of zeolites were tested: clinoptilolite and chabasite. The chabasite samples came from a quarry located in Grosseto, central Italy. The material had a grain size of 1–3 mm, a density of 0.7–0.9 $g{\cdot}cm^{-3}$, and a porosity (volume of voids over volume of bulk material) of 0.52–0.56. The clinoptilolite samples came from a quarry located in Arezzo, central Italy. The material had a grain size between 3 and 5 mm, a density of 0.6–0.8 $g{\cdot}cm^{-3}$, and a porosity of 0.45–0.5. The chemical composition of both materials is reported in Table S1 (Supplementary Material). Before their use, the zeolites were washed and dried for 4 h at 120 °C.

### 2.2. Analytical Methods Employed

CEC values reported in this work were provided by the material suppliers and had been determined using the methylthioninium chloride method [28]. Detailed information on solution composition, calibration procedure, and calculation equations was not available; therefore, these values are used only as complementary characterisation data. The cation composition of the zeolite samples was determined by inductive coupled plasma–optical emission spectroscopy analysis (ICP-OES) (Perkin Elmer Optima 2000 DV, Shelton, CT, USA). The significance of ICP-OES analysis lies in its capacity to ascertain the chemical composition of a given substance and to identify any impurities present [29]. The ICP-OES instrument was calibrated with a master individual standard (Sigma Aldrich, Darmstadt, Germany). The sensitivity of the instrument was 1 $\mu g \cdot L^{-1}$. The zeolite samples were previously ground in a Retsch ball mill at a frequency of 30 Hz for 3 min, then exposed to microwave acid attack (adding 2.5 mL of $H_2SO_4$ 96%, 2.5 mL of $H_3PO_4$ 85%, and 1 mL of HF 40%) [30]. Three replicates of the analysis were made using the microwave digestion system (Microwave Labstation MLS 1200, Milestone, Sorisole, Italy). Reagent blanks were run during ICP-OES analysis to ensure freedom from contamination. The crystalline structure of zeolite samples was identified by means of XRD analysis (D/tex Ultra 250 detector, Rigaku, Japan). Sorbent samples were manually crushed in a mortar to sub-mm size. The test was carried out using a 40 kV, 30 mA X-ray generator, applying a scan rate of 2° per minute, scan range 2θ. Phase identification was carried out with dedicated software (SmartLab Studio II), combined with the ICDD library. The specific area was determined with the Brunauer–Emmett–Teller (BET) method. Pore volume and the specific surface area of pores were obtained with the Gurvich rule (Tristar II Plus 3030 version 3.04, Micromeritics Instrument Corporation). This instrument defines adsorption isotherms with pure nitrogen at 77 K. Average repeatability of the BET instrument was ±1%. Prior to analysis, the zeolite samples were degassed at 300 °C for 4 h. BET specific surface areas were calculated from the adsorption isotherms using the relative pressure range $P/P_0$ = 0.01–0.30. Ion chromatography measurements were taken to measure chlorine concentration (Metrohm Eco IC, Herisau, Switzerland). Ammonium concentration was measured using measuring kits (Supelco Spectroquant Ammonium Test) and a spectrophotometer (UV31-scan, Onda, Carpi, Italy). The complete list of chemical reagents employed during the study is reported in the Supplementary Material.

### 2.3. Batch Adsorption Tests

Batch tests consisted of the introduction of a known mass of sample in a mixed reactor and, after the equilibrium time, measuring the contaminant concentration at equilibrium. For each sample, a mass of 10 g was introduced in 20 mm tubes. The tubes were filled with 50 mL of ammonia and de-ionised water solution with a known initial contaminant concentration (between 0.2 and 400 $mg \cdot L^{-1}$). The tubes were then inserted in a rotative mixer and stirred for 14 h to allow adsorption equilibrium to be approached. The temperature was 21 °C, and the stirring speed 8 rpm. Subsequently, the contaminant concentration in the liquid phase was measured. Two replicates of the analysis were run. The adsorption capacity $q_e$ was determined as a function of the equilibrium concentration in the aqueous phase (Equation (1)).

$$q_e = \frac{C_0 - C_{eq}}{m_{ad}} V, \quad (1)$$

where $C_{eq}$ is the contaminant concentration in the liquid phase at equilibrium, $C_0$ is the initial contaminant concentration in the liquid phase, $m_{ad}$ is the mass of adsorbent, and V is the solution volume. The obtained results were compared against the Langmuir and

Freundlich isotherm models. Matlab software (version R2025b) [31] was used for data fitting. The Langmuir isotherm model is represented by Equation (2):

$$q_e = \frac{\alpha\beta C_{eq}}{1 + \alpha C_{eq}}, \quad (2)$$

where α and β are empirical constants. The Freundlich isotherm model is represented by Equation (3):

$$q_e = kC_{eq}^{\frac{1}{N}}, \quad (3)$$

where k is the Freundlich capacity factor, and 1/N is the Freundlich intensity parameter.

### *2.4. Column Adsorption Tests*

Column adsorption tests were conducted according to the scheme shown in Figure 1. A polymethyl methacrylate column of height and diameter of 115 cm and 4.97 cm respectively was used. The column was filled with 500 g of adsorbent. The zeolite samples were first washed with ultrapure water, then dried for 1 h at 110 °C. Two gravel layers of 30 cm height, one at the top and one at the bottom of the column, were inserted to allow a uniform distribution of the flow. The column was operated as a closed system and the flow was directed upwards. The tests were designed to maintain flow conditions (fluid velocity) similar to those that might be found in a small decentralised wastewater treatment plant.

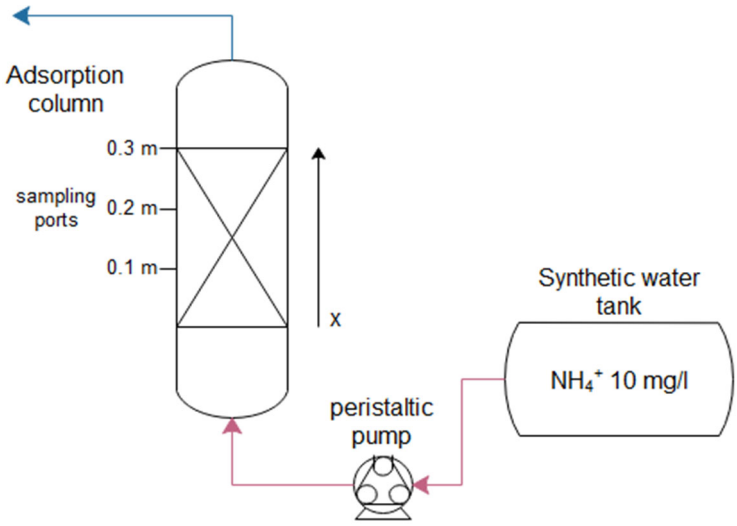



**Figure 1.** Configuration of column adsorption tests.

The experiment was conducted in three phases: conditioning, tracer test, and adsorption test. The conditioning phase served to remove any impurities from the material and achieve a steady-state flow distribution, resulting in complete saturation of the material pores. Initially, ultrapure water was pumped into the column until steady-state flow conditions were reached. When the outflow from the column was equal to the inlet flow, pumping was stopped. In the second phase, a tracing test was run, which served to characterise the hydraulic properties of the measurement system. In this test, a solution of de-ionised water and KCl was injected into the column, and the dispersion coefficient $D_L$ of the system was determined. The solution had a KCl concentration of 0.21 g·L$^{-1}$, corresponding to 95 ppm $Cl^-$. The tracer solution was pumped into the column at a flow $Q_{in}$ = 0.28 mL·s$^{-1}$. Electrical conductivity was measured inside the filling tank.

Every 15 min, a sample was taken, and conductivity was measured inside the sample tube. When the conductivity in the sample tube was equal to the conductivity in the tank, pumping was stopped. The concentration breakthrough curve was plotted. Measured

$Cl^-$ concentrations were fitted to the model (Equation (4)) to obtain the hydrodynamic dispersion coefficient $D_L$, and the effective velocity $v_e$. $D_L$ and $v_e$ were thus obtained from the conservative tracer tests and kept fixed during the fitting of ammonium breakthrough curves. In the third phase, the column was washed, then the actual adsorption test was carried out by injecting the ammonium solution at a known concentration. The initial ammonium concentration was 10 mg·$L^{-1}$. This value represents a residual concentration that could potentially be reached at the outlet of a small water treatment plant, for which tertiary treatment (e.g., filtration) would be necessary to remove it. Samples were taken at the top of the column (end of the adsorbent layer) every 2 h. The test lasted until the concentration measured at the column top was equal to the initial concentration. Two replicates of the analysis were run. The contaminant adsorption process was modelled with the differential equation reported in Equation (4). Equation (4) is based on the one-dimensional advection–dispersion equation including a retardation term and a first-order kinetic adsorption term. This model provides a physically based description of solute transport in porous media and accounts for the main mechanisms expected in the experimental columns, namely advection, hydrodynamic dispersion, adsorption, and mass-transfer limitations. The model assumes homogeneous flow conditions, constant transport parameters, negligible radial concentration gradients, and adsorption represented by a lumped first-order kinetic process.

$$R\frac{\partial C}{\partial t} = D_L\frac{\partial^2 C}{\partial x^2} - v_e\cdot\frac{\partial C}{\partial x} - kC \quad (4)$$

In Equation (4), R is the retardation coefficient, k is the kinetic constant, $D_L$ is the hydrodynamic dispersion coefficient, and $v_e$ is the effective velocity of the fluid. The kinetic coefficient k was considered an apparent lumped parameter describing non-equilibrium adsorption and possible mass-transfer limitations. The analytical solution for a semi-finite column, considering a step injection, is given by Equation (5):

$$C(x,t) = \frac{1}{2}C_0\exp\left(\frac{v_e x}{2D_l}\right)\cdot\left[\exp(-x\beta)erfc\frac{x - t\sqrt{(v_e/R)^2 + 4D_l k/R^2}}{2\sqrt{D_l t/R}} + \exp(x\beta)erfc\frac{x + t\sqrt{(v_e/R)^2 + \frac{4D_l k}{R^2}}}{2\sqrt{\frac{D_l t}{R}}}\right], \quad (5)$$

where x is the measurement height from the column bottom and $\beta^2 = \frac{v_e^2}{4D_l^2}$.

The adsorption capacity $q_t$ point was calculated as:

$$q_t = \frac{C_0 Q\int_0^t\left(1 - \frac{C}{C_0}\right)dt}{M} \quad (6)$$

where t is time (h), $C_0$ (mg·$L^{-1}$) is the initial influent ammonium concentration, C (mg·$L^{-1}$) is the effluent ammonium concentration at time t, M (g) is the mass of clinoptilolite in the column bed, and Q (L·$h^{-1}$) is the flow rate.

The experimental data-based breakthrough curve was also applied to the Thomas model. The Thomas model, represented by Equation (7), was selected because it is one of the most widely used models for analysing breakthrough curves in fixed-bed adsorption columns. It assumes plug-flow conditions and Langmuir-type adsorption kinetics and allows the estimation of adsorption capacity and apparent adsorption rate constants from experimental data. Although the model does not explicitly account for intraparticle diffusion or film mass-transfer resistance, it provides a useful and widely accepted ap-

proximation for comparing the performance of fixed-bed ammonium adsorption systems reported in the literature [32].

$$\frac{C_t}{C_0} = \frac{1}{1 + \exp\left(\frac{k_{Th} q_e M}{Q} - k_{Th} C_0 t\right)} \quad (7)$$

where $C_t$ and $C_0$ are the concentration of ammonia in the effluent at time t and the concentration of ammonia in the influent feed ($mg \cdot L^{-1}$), respectively; $k_{Th}$ is the model rate constant ($L \cdot h^{-1} \cdot mg^{-1}$); and M is the mass of clinoptilolite used in the column (mg). The model parameters were estimated using non-linear regression analysis [31].

## 3. Results

### *3.1. Characterisation Tests*

The results of the ICP-OES analysis are reported in Table 1. Table 1 shows the amounts of the main cations. The theoretical values of the cation exchange capacities, calculated from the cation composition resulting from the ICP-OES analysis, are 2.79 $meq \cdot g^{-1}$ and 3.71 $meq \cdot g^{-1}$ for clinoptilolite and chabasite, respectively [27]. The experimental CEC values were 1.80 ± 0.3 $meq \cdot g^{-1}$ and 3.25 ± 0.1 $meq \cdot g^{-1}$ for clinoptilolite and chabasite, respectively. The experimentally reported CEC values were lower than the theoretical capacities calculated from elemental composition. However, a detailed interpretation of this discrepancy is beyond the scope of the present study because the CEC analyses were performed externally and detailed testing conditions were not available [32].

**Table 1.** The results of the ICP-OES analysis.

| | **Chabasite** | | **Clinoptilolite** | |
|---|---|---|---|---|
| | **Element Content ($mol \cdot kg^{-1}$)** | **Si-Normalised** | **Element Content ($mol \cdot kg^{-1}$)** | **Si-Normalised** |
| Mg | 0.22 ± 0.003 | 0.037 | 0.16 ± 0.003 | 0.025 |
| Ca | 0.54 ± 0.170 | 0.090 | 0.29 ± 0.032 | 0.046 |
| Na | 0.18 ± 0.022 | 0.030 | 0.12 ± 0.009 | 0.019 |
| K | 0.82 ± 0.008 | 0.136 | 0.36 ± 0.007 | 0.057 |
| Si | 6.00 ± 0.036 | | 6.30 ± 0.399 | |
| Al | 2.60 ± 0.048 | | 1.61 ± 0.222 | |

The Si/Al ratio exerts a considerable influence on the material properties. A lower Si/Al ratio corresponds to higher ion exchange capacity. The Si/Al ratios of clinoptilolite and chabasite were 3.92 and 2.30, respectively. These values are in line with those reported in previous studies [33]. If normalised according to the silicon content, chabasite shows a higher cation content than clinoptilolite (Table 1).

XRD analyses were carried out on the clinoptilolite and chabasite samples to ascertain the degree of purity and to detect external solid phases. Phase quantification was performed by Rietveld refinement of the XRD patterns. The refinement quality indicators were Rp = 12% and Rwp = 15%. The diffractograms of the two zeolite samples are reported in Figures 2 and 3. For clinoptilolite, the spectrum analysis indicated that 93% of the composition was pure clinoptilolite, while for the remaining 7%, tridymite (6%) and cristobalite (<1%) were detected. For chabasite, 73% of the spectrum corresponded to pure chabasite, while sanidine (17%) and biotite (10%) were also detected (Tables 2 and 3).

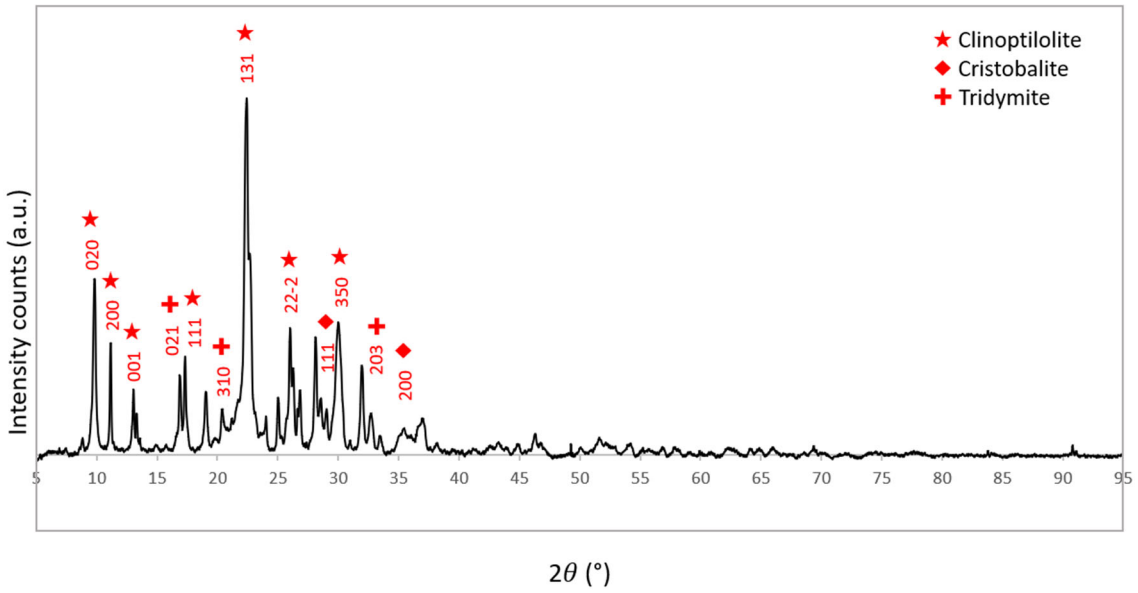



**Figure 2.** Diffractogram of clinoptilolite sample.

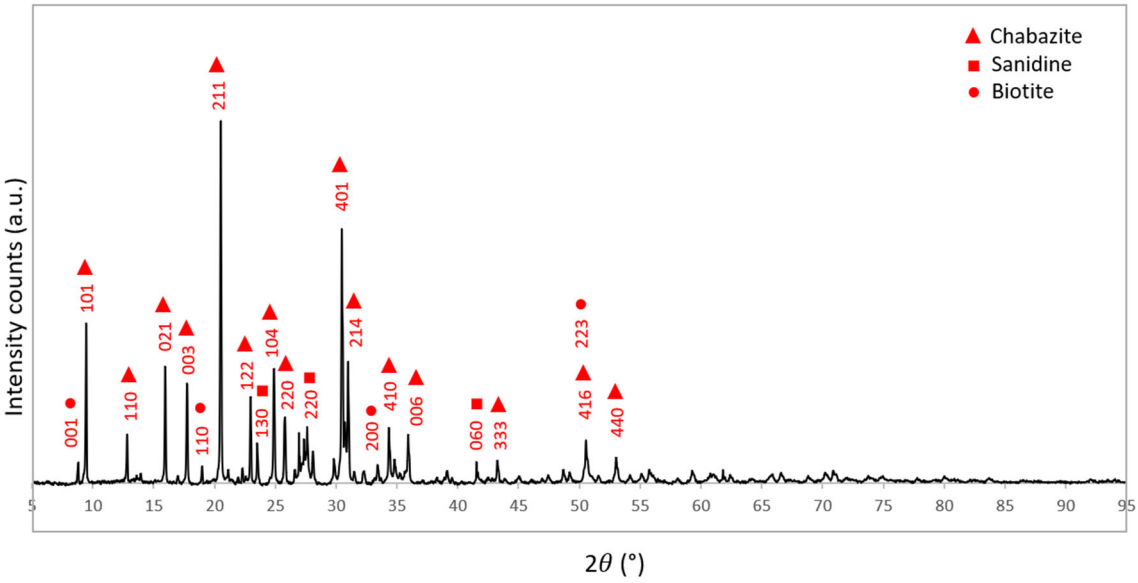



**Figure 3.** Diffractogram of chabasite sample.

**Table 2.** Description and references for clinoptilolite diffractogram.

| Mineral Phase | Peak Positions (2θ, °) | Reference |
|---|---|---|
| Clinoptilolite | 9.84, 22.33, 22.46 | [34] |
| Cristobalite | 21.94, 31.66, 36.05 | [35] |
| Tridymite | 20.5, 21.67, 23.22 | [36] |

**Table 3.** Description and references for chabasite diffractogram.

| Mineral Phase | Peak Positions (2θ, °) | Reference |
|---|---|---|
| Chabasite | 9.47, 20.54, 30.52 | [37] |
| Sanidine | 23.52, 26.93, 27.61 | [38] |
| Biotite | 8.74, 26.42, 33.95 | [39] |

The adsorption and desorption isotherms with pure nitrogen at 77 K are reported in Figures 4 and 5. For clinoptilolite, the isotherm shows distinct adsorption and desorption curves, forming a marked hysteresis in the relative pressure ($P/P_0$) region between approximately 0.4 and 0.9. A very rapid increase in adsorbed volume is also visible near $P/P_0 = 1$, indicating capillary condensation in mesoporous or macroporous pores. The overall shape of the curve suggests behaviour typical of a mesoporous material, with a minimal contribution from microporosity (almost flat initial zone for $P/P_0 < 0.1$). Adsorption and desorption diverge gradually, not sharply, indicating the presence of lamellar particle aggregates or slit-like pores (open or not completely cylindrical pores). For chabasite, the adsorption and desorption curves are almost superimposed, with limited hysteresis. The adsorbed amount increases rapidly at low relative pressures ($P/P_0 < 0.05$) and then tends towards an almost horizontal plateau, indicating that most adsorption sites become readily saturated. No marked increase is observed for $P/P_0 > 0.9$, indicating that the presence of both mesopores and macropores is limited. The isotherm indicates a microporous material with uniform pores. The average specific BET areas measured with the porosimeter were 29.9 $m^2 \cdot g^{-1}$ and 291.6 $m^2 \cdot g^{-1}$ for clinoptilolite and chabasite, respectively. The pore volume and specific surface area of pores obtained with the Gurvich rule are reported in the Supplementary Material (Figures S1–S4). The total pore volumes were 0.12 $cm^3 \cdot g^{-1}$ and 0.20 $cm^3 \cdot g^{-1}$ for clinoptilolite and chabasite, respectively. These values are in accordance with previous studies [40].

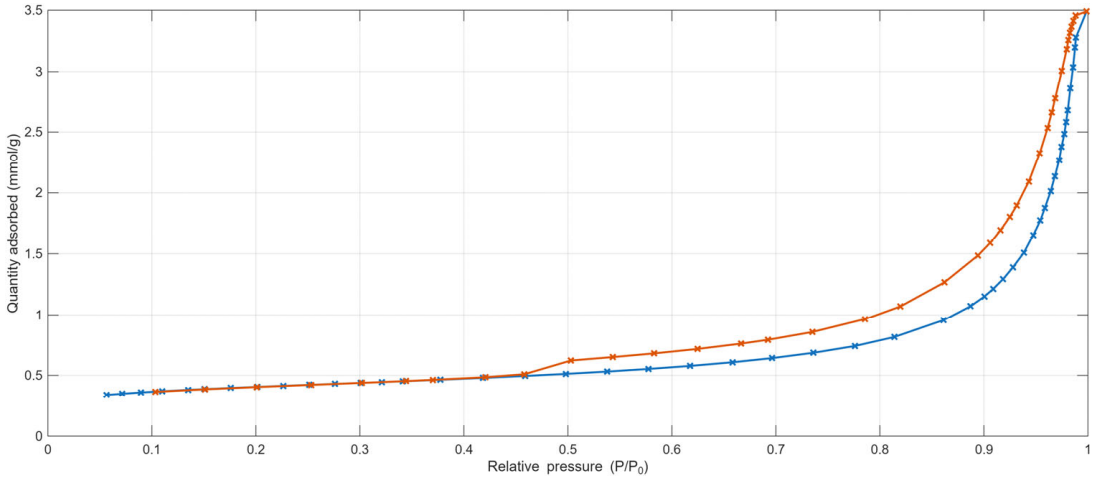



**Figure 4.** Adsorption (blue) and desorption (orange) isotherms for clinoptilolite with pure nitrogen at 77 K.

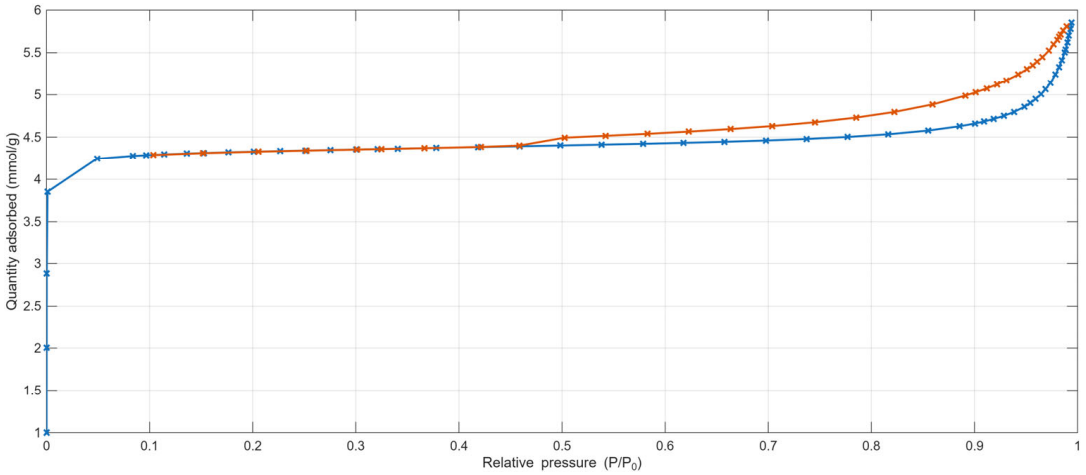



**Figure 5.** Adsorption (blue) and desorption (orange) isotherms for chabasite with pure nitrogen at 77 K.

### *3.2. Batch Test Results*

The results of batch adsorption tests for ammonium are presented in Figure 6. Two replicate runs were done. Figure 6 shows that clinoptilolite has a higher adsorption capacity than chabasite; the values of $q_e$ for $C_{eq}$ = 10 mg·L$^{-1}$ are 1.66 ± 0.08 mg·g$^{-1}$ and 1.47 ± 0.03 mg·g$^{-1}$ for clinoptilolite and chabasite, respectively. The pH of the batch test solutions was measured and was approximately 6.7 ± 0.02. The experimental measures were compared with the Langmuir and Freundlich models. The results of this fitting, reported in Table S2 (Supplementary Material) and Figure 6, show that both models behave similarly. The Freundlich isotherm afforded a better correlation coefficient for data fitting ($R^2$ = 0.99; Table S2, Supplementary Material). Thus, the experimental data for both clinoptilolite and chabasite were satisfactorily represented by the Freundlich model. The best fit of the Freundlich model indicates that the surface of the materials is not homogeneous and there are sites with different adsorption energies. Furthermore, adsorption does not stop at a monolayer but can proceed over multiple layers. Comparing the two adsorbents, generally a higher value of the n coefficient has been reported in the literature [33].

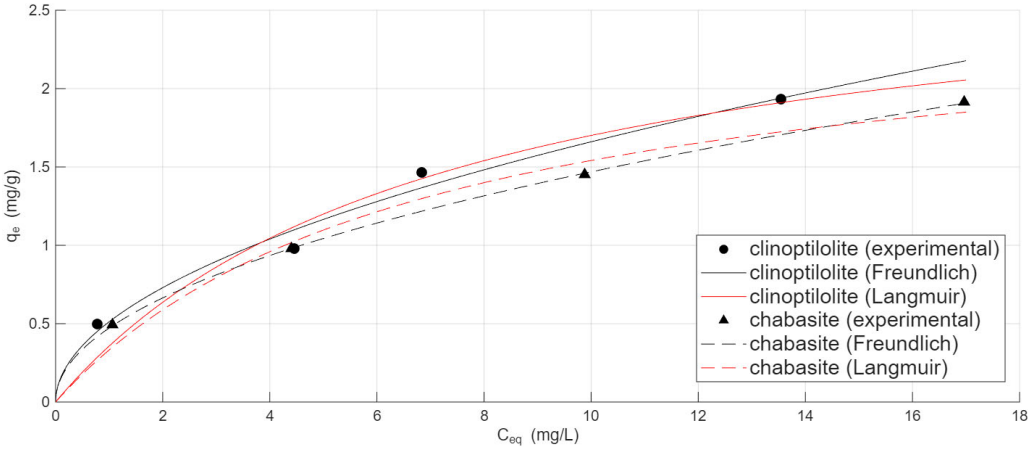



**Figure 6.** Adsorption isotherms for clinoptilolite and chabasite at 21 °C.

Adsorption thermodynamics studies can reveal internal energy changes during the adsorption process. The standard free energy change (ΔG°) can be calculated using Equation (8):

$$\Delta G^0 = -RTlnK_d \quad (8)$$

where R is the universal gas constant (8.314 J·mol$^{-1}$·K$^{-1}$), T is the absolute temperature (K), and $K_d$ is the adsorption coefficient. $K_d$ is calculated as (Equation (9)):

$$K_d = \frac{C_0 - C_e}{C_e} \frac{V}{M} \quad (9)$$

where V is the volume of the solution, and M is the mass of zeolite. The adsorption equilibrium constant was extrapolated by plotting ln $K_d$ vs. $C_e$ and extrapolating $C_e$ to 0.

### *3.3. Column Adsorption Tests*

Through the tracer test, the effective velocity $v_e$ and the dispersion coefficient $D_L$ were determined. For clinoptilolite, $v_e = 2.4 \cdot 10^{-4}$ m·s$^{-1}$, and $D_L = 2.3 \cdot 10^{-6}$ m$^2$·s$^{-1}$. For chabasite, $v_e = 1.5 \cdot 10^{-4}$ m·s$^{-1}$, and $D_L = 3.3 \cdot 10^{-6}$ m$^2$·s$^{-1}$. The ammonium adsorption column test lasted approximately 500 h for clinoptilolite and 650 h for chabasite. Two replicates were run. The initial ammonium concentration $C_0$ was 10 mg·L$^{-1}$. The pH of the solution was measured before the tests, and it was 6.7 ± 0.02. The pH at the end of the tests

had not changed compared to the initial value. The empty bed contact time (EBCT) was approximately 63.5 min. No significant head loss increase or clogging phenomena were observed during the experiments. The concentration breakthrough curve is reported in Figure 7. The graph reports the ammonium concentration trend at three distinct column positions (x = 0.1 m, x = 0.2 m, x = 0.3 m).

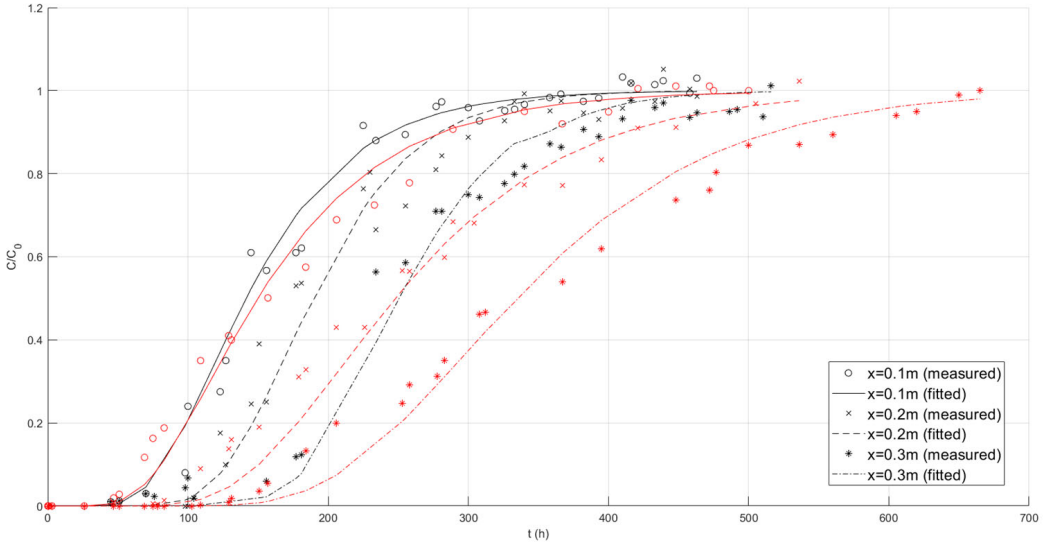



**Figure 7.** The breakthrough curves of the column adsorption test for ammonium with clinoptilolite (black) and chabasite (red).

At the column bottom (x = 0.1), the breakpoints ($C/C_0 = 0.1$) of ammonia occurred at around 98 h and 69 h for clinoptilolite and chabasite respectively. The column exhaustions ($C/C_0 = 0.9$) were observed after 255 h and 289 h for clinoptilolite and chabasite respectively.

Fitting curves derived from Equation (5) are displayed Figure 7. The model fitting was generated by varying the retardation factor R according to the lowest possible residual from the experimental data. The resulting values of R are reported in Table 4. R was in the range 742–1334 for clinoptilolite and 515–534 for chabasite. The value of R decreased with increasing column height, probably due to the slight decreasing pressure with increasing height in the column.

**Table 4.** Retardation factor at different column sampling heights.

| Column Position x (m) | Retardation Factor R | |
|---|---|---|
| | **Clinoptilolite** | **Chabasite** |
| 0.1 | 1334 | 534 |
| 0.2 | 852 | 520 |
| 0.3 | 742 | 515 |

Figure 7 also shows that the breakthrough phase is very slight, and that it takes a long time to reach the breakthrough point, indicating that the column design could be improved [41].

Complete material saturation was reached after 450 h and 650 h for clinoptilolite and chabasite, respectively (x = 0.3 m). The ammonia uptake capacities at saturation calculated with the Thomas model (x = 0.3 m) are reported in Table 5. These values are close to the experimentally determined column capacities of $2.48 \pm 0.3$ mg·g$^{-1}$ and $2.21 \pm 0.2$ mg·g$^{-1}$. The number of treated bed volumes at breakthrough was approximately

93 and 65 for clinoptilolite and chabasite, respectively, while column exhaustion occurred after approximately 425 and 614 bed volumes.

**Table 5.** Fitting parameters with the Thomas model.

| Sample | Parameter | Estimate | SE | Adjusted $R^2$ |
|---|---|---|---|---|
| Clinoptilolite | $q_{e,Th}$ | 2.37 | 0.06 | 0.985 |
| | $k_{Th}$ | $1.8 \cdot 10^{-3}$ | $1.2 \cdot 10^{-4}$ | |
| Chabasite | $q_{e,Th}$ | 2.19 | 0.04 | 0.986 |
| | $k_{Th}$ | $2.8 \cdot 10^{-3}$ | $2.0 \cdot 10^{-4}$ | |

Free energy changes calculated with Equations (8) and (9) were $-1760$ J·mol$^{-1}$ for clinoptilolite, and $-1345$ J·mol$^{-1}$ for chabasite. Negative $\Delta G^{\circ}$ values indicate that the adsorption processes are spontaneous.

## 4. Discussion

Zeolites are commonly used in various applications due to their high cation exchange capacity and high surface area. The efficiency of these materials is highly dependent on the nature of the contaminant. Zeolite performance of ammonium adsorption in both batch and column tests has been reported on extensively. However, the direct comparison of adsorption efficiency of various zeolite types is not straightforward, due to variable experimental settings. The dosage of zeolite, concentration of ammonia, and contact time are key determinants of adsorption [42]. In addition, the majority of previous studies have reported adsorption capacities which are related to higher equilibrium concentrations and/or higher adsorbent dosage. In an extensive review conducted by Shoumkova [43], ammonium adsorption capacities between 1.3 mg·g$^{-1}$ and 21.7 mg·g$^{-1}$ were reported. Additional and updated results of both batch and column experiments were also reported by [20]. Fu et al. [44] reported an equilibrium adsorption capacity of 4.29 mg·g$^{-1}$ for a clinoptilolite having a BET surface area of 31.6 m$^2$·g$^{-1}$, very similar to that of the present study. Modifying the natural samples allowed an increased $q_{max}$, up to 16.96 mg·g$^{-1}$ (Table 6).

**Table 6.** Comparison of ammonium adsorption capacities reported for natural and modified zeolites.

| Reference | Zeolite | Modification | Test Type | Initial $NH_4^+$ Concentration, $C_0$ (mg L$^{-1}$) | Adsorption Capacity, q (mg g$^{-1}$) |
|---|---|---|---|---|---|
| This study | Clinoptilolite | None | Batch | 10 | 1.66 |
| This study | Chabasite | None | Batch | 10 | 1.47 |
| This study | Clinoptilolite | None | Column | 10 | 2.48 |
| This study | Chabasite | None | Column | 10 | 2.21 |
| [38] | Clinoptilolite | None | Batch | 5 | 4.29 |
| [38] | Clinoptilolite | $NaNO_3$-modified | Batch | 5 | 16.96 |
| [33] | Clinoptilolite | None | Column | 400 | 15.8 |
| [43] | Various natural zeolites | Various | Batch/Column | Variable | 1.3–21.7 |

The evaluation of the experimental tests conducted on the zeolite samples in this study provides more insights on ammonium adsorption. The initial ammonium concentration was limited to 10 mg·L$^{-1}$ to assess absorption capacity at low concentrations, in order to

evaluate the use of these natural materials in low-cost filtration systems, which could also be applied in decentralised treatment plants. Thus, the tests were designed to focus on low initial concentration rather than finding maximum absorption capacity.

The results of the column tests show an overall material lifetime between 450 and 650 h before complete saturation ($C/C_0 = 0.9$). This is considered a promising value for the purpose of their potential use in small filtration systems. The results confirm that clinoptilolite and chabasite show good affinity with ammonium. It should be noted that both the first-order kinetic term and the Thomas model provide simplified descriptions of ammonium ion exchange on natural zeolites. They do not explicitly account for competitive exchange with background cations, intraparticle diffusion, or spatial heterogeneity of adsorption sites. Therefore, the fitted parameters should be regarded as apparent parameters valid under the experimental conditions adopted in this study.

The adsorption capacity reported in other studies on unmodified materials, when referring to a low initial ammonium concentration ($C_0 < 10$ mg·L$^{-1}$), has generally been higher, sometimes as high as 20 mg·g$^{-1}$ [40,45]. However, these studies are difficult to compare to the present one as the experimental conditions in those studies were not fully specified, especially the cation exchange capacity of the materials or the flow rate of the aqueous solution into the adsorbent column. A comparison can be made, though, on the retardation factor. In this study, the retardation factor was found to be in the ranges 742–1334 for clinoptilolite and 515–534 for chabasite. In a study by [40], retardation factors in the range 979–1107 were found for ammonium adsorption with clinoptilolite. Considering the above results, modifying the material physically or chemically could certainly contribute to greater efficiency, even if this would entail additional costs [46].

Looking at the materials considered, it is difficult to clearly define the governing mechanism for adsorption. Ion exchange is considered the dominant mechanism responsible for ammonium removal by both zeolitic materials [19]. However, the experimental results of this study showed that clinoptilolite showed better performance than chabasite. This is in contrast with previous findings, in which chabasite was found to show higher adsorption capacity. The adsorption capacities found do not reflect the difference in specific surface area, which is about 10 times higher for chabasite than for clinoptilolite. Nor can the difference in the CEC or Si-normalised cation content explain the results (Table 1).

One factor that can certainly influence this is the purity of the material (73% for chabasite and 93% for clinoptilolite), identified by the XRD analyses. The presence of sanidine and biotite in the chabasite sample may have reduced the effective amount of active zeolitic material, acting mainly as inert diluents. However, when normalised for purity, the adsorption capacity of chabasite remains lower than that of clinoptilolite. This suggests that additional factors influenced adsorption performance. The $N_2$ adsorption isotherms indicate that the clinoptilolite-rich material exhibited a significant mesoporous textural contribution, whereas the chabasite-rich material showed a stronger microporous character. These observations reflect the overall texture of the natural zeolite-bearing rocks rather than the intrinsic pore architecture of the pure zeolite crystal structures. Such textural differences may influence intraparticle diffusion and the accessibility of exchange sites. The larger pores observed in clinoptilolite may facilitate ammonium transport within the adsorbent particles and promote faster attainment of equilibrium, whereas the narrower pore network of chabasite may result in greater diffusion resistance. Although direct kinetic measurements were not performed, this interpretation is consistent with the breakthrough behaviour observed in the column tests and provides a plausible explanation for the higher adsorption performance of clinoptilolite despite its lower BET surface area and CEC [47,48]. A factor complementary to the slow kinetics is probably the low initial concentration, which determines a limited driving force for the exchange. However, this interpretation remains

a hypothesis and should be verified through dedicated kinetic and mass-transfer studies. Such studies should also include the improvement of regression fitting of the adsorption isotherms [49].

An additional factor that may have contributed to the observed behaviour is the different commercial granule size of the two materials (1–3 mm for chabasite and 3–5 mm for clinoptilolite). While such differences are not expected to substantially affect the intrinsic pore structure measured by $N_2$ physisorption, they may influence mass-transfer rates and intraparticle diffusion during adsorption experiments. Nevertheless, the marked differences observed in BET surface area, pore volume, and adsorption isotherm shape are more likely attributable to the different mineralogical structures and pore architectures of the two zeolites [50].

Another factor to consider is the acidity of the solution, which is also known to affect the adsorption performance of zeolites [51]. The pH measurements showed that, in this study, a constant value of $6.7 \pm 0.02$ was maintained during the tests. At this pH value, the equilibrium between ionised and un-ionised forms of ammonia is clearly shifted towards the ionised form [52]. Nitrogen was therefore present in the ammonium form, and thus readily available for the cation exchange process with the adsorbent. Thus, it is expected that the acidity of the solution had no significant contribution in this study. Analysing the effect of pH on adsorption, however, is an important factor currently addressed by other scholars, and it should be further investigated in future tests [44].

The present study has some limitations that should be acknowledged. The adsorption experiments were conducted using synthetic ammonium solutions under controlled laboratory conditions. The effects of competing ions, dissolved organic matter, and suspended solids commonly present in real wastewaters were not investigated. In addition, the study focused on single-pass adsorption experiments and did not evaluate regeneration, reuse, or long-term ageing of the adsorbents. The presence of competing cations could significantly affect the ammonium removal from water through cation exchange, especially in the presence of potassium. Competing cations could bring to low fresh water specific productivity and frequent regenerations of the adsorbent [53,54]. The feasibility of low-cost filtration systems based on the use of zeolites will also depend on the possibility of recovering the adsorbent material. In this regard, various options are currently being studied, including the biological or ion exchange-based regeneration of the material, or non-regenerative approaches based on the use of spent material in agriculture [53,55]. Although natural zeolites are generally regarded as environmentally safe materials, exhausted adsorbents may release retained ammonium if improperly managed. Therefore, regeneration, reuse, or controlled disposal should be considered to minimise potential environmental impacts.

The experimentally determined breakthrough times and adsorption capacities may be used as preliminary design parameters for estimating filter dimensions and media replacement frequency in decentralised treatment systems. However, full-scale design would require additional information on wastewater composition, hydraulic loading, competing ions, and regeneration strategy. The decision to design a removal system based on this approach will depend on both technical and economic factors, which will need to be assessed on a case-by-case basis. A detailed economic assessment was beyond the scope of this study. However, natural zeolites are generally less expensive than engineered adsorbents because they require limited processing and are widely available. Their potential application in decentralised wastewater treatment therefore appears promising, although future studies should evaluate regeneration performance and life-cycle costs under real operating conditions. In-depth experimental studies, supported by advanced data collection and elaboration, could support this research [56,57].

## 5. Conclusions

This study proposed the characterisation and comparison of natural zeolites for ammonium removal from water at low initial concentration (10 $mg \cdot L^{-1}$ for column tests). Given the observed saturation dynamics, the use of these materials seems applicable, especially in the context of sustainable low-cost purification technologies for developing countries. Nevertheless, the adsorption capacity of the tested samples was lower than the average values previously found for chemically or physically modified sorbents. The comparison between clinoptilolite and chabasite showed contrasting results with respect to previous studies. Although it is difficult to clearly define the leading mechanism for adsorption, the difference in the behaviour of the two materials is probably to be found in the analysis of the pores and the kinetics of the exchange process. The microporous nature of the chabasite sample may imply higher diffusive resistance resulting in slower penetration of the contaminant molecules inside the material. The purity of the material (17% of sanidine was found in chabasite samples) may also have contributed to these results. Future studies should focus on the quantification of adsorption kinetics, intraparticle diffusion, and mass-transfer limitations under both batch and dynamic conditions. Particular attention should be devoted to understanding how pore structure (microporous versus mesoporous characteristics) influences ammonium transport, accessibility of exchange sites, and overall adsorption performance at low ammonium concentrations. For the purpose of possible applications, this study's detailed characterisation of the material seems appropriate. Future applicative studies should be addressed to test these materials under real operating conditions. Adsorption capacity with real wastewater could be significantly different from the values obtained, depending on environmental conditions, the presence of suspended solids, pH, and possible trap-door effects. The decision to design a removal system based on zeolite adsorption will depend on both technical and economic factors, which will need to be assessed on a case-by-case basis. However, such a design will not overlook basic sustainability principles, including circular economy, BAT techniques, and the "near-zero discharge" of hazardous wastes. From a circular economy perspective, ammonium-saturated zeolites may be regenerated through ion exchange treatments and reused in adsorption processes. Alternatively, because of the retained nitrogen content, they could be valorised as slow-release fertilisers or soil amendments, provided that no harmful contaminants are present.

**Supplementary Materials:** The following supporting information can be downloaded at https://www.mdpi.com/article/10.3390/su18136396/s1.

**Author Contributions:** Conceptualization: M.R. and M.Z.; data curation: M.R. and E.M.; formal analysis: M.R., E.M. and M.Z.; funding acquisition: M.Z.; investigation: M.R., E.M. and M.Z.; methodology: M.R. and M.Z.; project administration: M.R. and M.Z.; resources: M.R. and M.Z.; software: M.R. and E.M.; supervision: M.R. and M.Z.; validation: M.R. and M.Z.; visualisation: M.R., E.M. and M.Z.; writing—original draft: M.R. and E.M.; writing—review and editing: M.R., E.M. and M.Z. All authors have read and agreed to the published version of the manuscript.

**Funding:** This study was carried out within the framework of the project "Supporting OWSSB (India) in Upgrading Capacities in Wastewater and Faecal Sludge Management (SO-WOP)", funded by the United Nations Human Settlements Programme.

**Institutional Review Board Statement:** Not applicable.

**Informed Consent Statement:** Not applicable.

**Data Availability Statement:** The authors are available to share the data used for this study, but suggest that they be contacted in advance so that they can explain how the data is organised and how to use it correctly.

**Acknowledgments:** The authors would like to acknowledge Giovanna Zanetti and Camila Mori de Oliveira for their valuable contribution to the experimental activities.

**Conflicts of Interest:** The authors declare no conflicts of interest.

## References

1. Ravina, M.; Galletta, S.; Dagbetin, A.; Kamaleldin, O.A.H.; Mng'ombe, M.; Mnyenyembe, L.; Shanko, A.; Zanetti, M. Urban Wastewater Treatment in African Countries: Evidence from the Hydroaid Initiative. *Sustainability* **2021**, *13*, 12828. [CrossRef]
2. De Magalhães, L.F.; Da Silva, G.R.; Peres, A.E.C. Zeolite Application in Wastewater Treatment. *Adsorpt. Sci. Technol.* **2022**, *2022*, 4544104. [CrossRef]
3. Sprynskyy, M.; Lebedynets, M.; Terzyk, A.P.; Kowalczyk, P.; Namieśnik, J.; Buszewski, B. Ammonium Sorption from Aqueous Solutions by the Natural Zeolite Transcarpathian Clinoptilolite Studied under Dynamic Conditions. *J. Colloid Interface Sci.* **2005**, *284*, 408–415. [CrossRef] [PubMed]
4. Novembre, D.; Gimeno, D.; Calista, M.; Mancinelli, V.; Miccadei, E. On the Suitability of Phillipsite-Chabazite Zeolitite Rock for Ammonia Uptake in Water: A Case Study from the Pescara River (Italy). *Sci. Rep.* **2022**, *12*, 9284. [CrossRef] [PubMed]
5. Farghali, M.; Chen, Z.; Osman, A.I.; Ali, I.M.; Hassan, D.; Ihara, I.; Rooney, D.W.; Yap, P.-S. Strategies for Ammonia Recovery from Wastewater: A Review. *Environ. Chem. Lett.* **2024**, *22*, 2699–2751. [CrossRef]
6. Li, L.; Liu, Y.; Gui, X.; Zhou, B.; Xing, Z.; Ke, X.; Yuan, J.; Zhao, T. Size-Dependent Regulation of Iron Transport and Nitrogen Metabolism by Nanoscale Zero-Valent Iron in Heterotrophic Nitrifying–Aerobic Denitrifying Bacteria. *Bioresour. Technol.* **2026**, *449*, 134383. [CrossRef] [PubMed]
7. Hasan, M.N.; Altaf, M.M.; Khan, N.A.; Khan, A.H.; Khan, A.A.; Ahmed, S.; Kumar, P.S.; Naushad, M.; Rajapaksha, A.U.; Iqbal, J.; et al. Recent Technologies for Nutrient Removal and Recovery from Wastewaters: A Review. *Chemosphere* **2021**, *277*, 130328. [CrossRef] [PubMed]
8. Wu, M.; Zhao, P.; Song, W.; Wang, X. Simultaneous pH Regulation and Fouling Mitigation in Anaerobic Acidification Membrane Bioreactors Using NaOH Backwashing: Performance and Mechanistic Insights. *J. Membr. Sci.* **2026**, *747*, 125310. [CrossRef]
9. Borzooei, S.; Campo, G.; Cerutti, A.; Meucci, L.; Panepinto, D.; Ravina, M.; Riggio, V.; Ruffino, B.; Scibilia, G.; Zanetti, M. Feasibility Analysis for Reduction of Carbon Footprint in a Wastewater Treatment Plant. *J. Clean. Prod.* **2020**, *271*, 122526. [CrossRef]
10. Li, Y.; Bu, J.; Sun, Y.; Huang, Z.; Zhu, X.; Li, S.; Chen, P.; Tang, Y.; He, G.; Zhong, S. Efficient Degradation of Norfloxacin by Synergistic Activation of PMS with a Three-Dimensional Electrocatalytic System Based on Cu-MOF. *Sep. Purif. Technol.* **2025**, *356*, 129945. [CrossRef]
11. Jasim, N.A. The Design for Wastewater Treatment Plant (WWTP) with GPS X Modelling. *Cogent Eng.* **2020**, *7*, 1723782. [CrossRef]
12. Rout, P.R.; Shahid, M.K.; Dash, R.R.; Bhunia, P.; Liu, D.; Varjani, S.; Zhang, T.C.; Surampalli, R.Y. Nutrient Removal from Domestic Wastewater: A Comprehensive Review on Conventional and Advanced Technologies. *J. Environ. Manag.* **2021**, *296*, 113246. [CrossRef] [PubMed]
13. Liu, H.; Liang, L.; Tian, F.; Xi, X.; Zhang, Y.; Zhang, P.; Cao, X.; Bai, Y.; Zhang, C.; Dong, L. Scalable Preparation of Ultraselective and Highly Permeable Fully Aromatic Polyamide Nanofiltration Membranes for Antibiotic Desalination. *Angew. Chem. Int. Ed.* **2024**, *63*, e202402509. [CrossRef] [PubMed]
14. Dehmani, Y.; Ba Mohammed, B.; Oukhrib, R.; Dehbi, A.; Lamhasni, T.; Brahmi, Y.; El-Kordy, A.; Franco, D.S.P.; Georgin, J.; Lima, E.C.; et al. Adsorption of Various Inorganic and Organic Pollutants by Natural and Synthetic Zeolites: A Critical Review. *Arab. J. Chem.* **2024**, *17*, 105474. [CrossRef]
15. Guo, L.; Chen, W.; Wang, C.; Dong, B. Application of Electrochemically Assisted Synthesis of MOFs-Derived Phosphides as Catalyst for $CH_4$-$CO_2$ Reforming. *Int. J. Electrochem. Sci.* **2023**, *18*, 26–32. [CrossRef]
16. Inglezakis, V.J. The Concept of "Capacity" in Zeolite Ion-Exchange Systems. *J. Colloid Interface Sci.* **2005**, *281*, 68–79. [CrossRef] [PubMed]
17. Chaves Lima, R.; Bieseki, L.; Vinaches Melguizo, P.; Castellã Pergher, S.B. *Environmentally Friendly Zeolites: Synthesis and Source Materials*; Engineering Materials; Springer International Publishing: Cham, Switzerland, 2019.
18. Gonzalez-Olmos, R.; Gutierrez-Ortega, A.; Sempere, J.; Nomen, R. Zeolite versus Carbon Adsorbents in Carbon Capture: A Comparison from an Operational and Life Cycle Perspective. *J. $CO_2$ Util.* **2022**, *55*, 101791. [CrossRef]
19. Pavelić, K.; Hadžija, M.; Bedrica, L.; Pavelić, J.; Đikić, I.; Katić, M.; Kralj, M.; Bosnar, M.H.; Kapitanović, S.; Poljak-Blaži, M.; et al. Natural Zeolite Clinoptilolite: New Adjuvant in Anticancer Therapy. *J. Mol. Med.* **2001**, *78*, 708–720. [CrossRef] [PubMed]
20. Manoharmayum, V.S.; Ningombam, D. Zeolites as Versatile Material for Sustainable Water Purification: A Review. *EQA Int. J. Environ. Qual.* **2024**, *65*, 25–34. [CrossRef] [PubMed]

21. Boles, J.R. Review of Natural Zeolites: Occurrence, Properties, Applications: Editors: D.L. Bish and D.W. Ming. Reviews in Mineralogy and Geochemistry, Volume 45, Mineralogical Society of America, 1015 Eighteenth Street NW, Suite 601, Washington, D.C. 20036-5274, U.S.A. 2001, 654 p. US $24 for MSA and GS Members; US $32 for Others. ISBN0-939950-57-X. *Can. Mineral.* **2002**, *40*, 1521–1522. [CrossRef]
22. Li, J.; Gao, M.; Yan, W.; Yu, J. Regulation of the Si/Al Ratios and Al Distributions of Zeolites and Their Impact on Properties. *Chem. Sci.* **2023**, *14*, 1935–1959. [CrossRef] [PubMed]
23. Rodríguez-Iznaga, I.; Shelyapina, M.G.; Petranovskii, V. Ion Exchange in Natural Clinoptilolite: Aspects Related to Its Structure and Applications. *Minerals* **2022**, *12*, 1628. [CrossRef]
24. Qiu, W.; Zheng, Y. Removal of Lead, Copper, Nickel, Cobalt, and Zinc from Water by a Cancrinite-Type Zeolite Synthesized from Fly Ash. *Chem. Eng. J.* **2009**, *145*, 483–488. [CrossRef]
25. Adam, M.R.; Othman, M.H.D.; Hubadillah, S.K.; Abd Aziz, M.H.; Jamalludin, M.R. Application of Natural Zeolite Clinoptilolite for the Removal of Ammonia in Wastewater. *Mater. Today Proc.* 2023; *in press*. [CrossRef]
26. Byrappa, K.; Yoshimura, M. Hydrothermal Synthesis and Growth of Zeolites. In *Handbook of Hydrothermal Technology*; Elsevier: Amsterdam, The Netherlands, 2013; pp. 269–347.
27. Das, D.; Sengupta, S. Alkaline Hydrothermal Treatment of Chabazite to Enhance Its Ammonium Removal and Recovery Capabilities through Recrystallization. *Processes* **2023**, *12*, 85. [CrossRef]
28. Khoualdia, B.; Loungou, M.; Elaloui, E. Adsorption of Organic Matter from Industrial Phosphoric Acid ($H_3PO_4$) onto Activated Bentonite. *Arab. J. Chem.* **2017**, *10*, S1073–S1080. [CrossRef]
29. Huang, J.; Lyu, H.; Wang, C.; Su, X.; Dong, W.; Wan, Y.; Song, T.; Shen, X. Residual NAPL Intermittent Expulsion with Increasing Freeze–Thaw Cycles in Saturated Porous Media: Findings from a 2.5-D Microfluidic Platform. *Water Resour. Res.* **2026**, *62*, e2025WR042230. [CrossRef]
30. Müller, E.I.; Mesko, M.F.; Moraes, D.P.; Korn, M.D.G.A.; Flores, É.M.M. Wet Digestion Using Microwave Heating. In *Microwave-Assisted Sample Preparation for Trace Element Analysis*; Elsevier: Amsterdam, The Netherlands, 2014; pp. 99–142.
31. Mathworks Inc. *Matlab, R2025b*; Mathworks Inc.: Natick, MA, USA, 2025.
32. Eberle, S.; Schmalz, V.; Börnick, H.; Stolte, S. Natural Zeolites for the Sorption of Ammonium: Breakthrough Curve Evaluation and Modeling. *Molecules* **2023**, *28*, 1614. [CrossRef] [PubMed]
33. Damodara Kannan, A.; Parameswaran, P. Ammonia Adsorption and Recovery from Swine Wastewater Permeate Using Naturally Occurring Clinoptilolite. *J. Water Process Eng.* **2021**, *43*, 102234. [CrossRef]
34. Koyama, K.; Takeuchi, Y. Clinoptilolite: The Distribution of Potassium Atoms and Its Role in Thermal Stability. *Z. Für Krist. Cryst. Mater.* **1977**, *145*, 216–239. [CrossRef]
35. Peacor, D.R. High-Temperature Single-Crystal Study of the Cristobalite Inversion. *Z. Für Krist.* **1973**, *138*, 274–298. [CrossRef]
36. Kihara, K.; Matsumoto, T.; Imamura, M. Structural Change of Orthorhombic-I Tridymite with Temperature: A Study Based on Second-Order Thermal-Vibrational Parameters. *Z. Für Krist. Cryst. Mater.* **1986**, *177*, 27–38. [CrossRef]
37. Nakatsuka, A.; Okada, H.; Fujiwara, K.; Nakayama, N.; Mizota, T. Crystallographic Configurations of Water Molecules and Exchangeable Cations in a Hydrated Natural CHA-Zeolite (Chabazite). *Microporous Mesoporous Mater.* **2007**, *102*, 188–195. [CrossRef]
38. Yamnova, N.A.; Khomyakov, A.P.; Zlykhenskaya, I.V. Refinement of the Crystal Structure of Sanidine-like Feldspar. *Crystallogr. Rep.* **2000**, *45*, 754–758. [CrossRef]
39. Brigatti, M.F.; Guidotti, C.V.; Malferrari, D.; Sassi, F.P. Single-Crystal X-Ray Studies of Trioctahedral Micas Coexisting with Dioctahedral Micas in Metamorphic Sequences from Western Maine. *Am. Mineral.* **2008**, *93*, 396–408. [CrossRef]
40. Ho, Y.S.; McKay, G. Pseudo-Second Order Model for Sorption Processes. *Process Biochem.* **1999**, *34*, 451–465. [CrossRef]
41. Vukojević Medvidović, N.; Perić, J.; Trgo, M.; Mužek, M.N. Removal of Lead Ions by Fixed Bed of Clinoptilolite–The Effect of Flow Rate. *Microporous Mesoporous Mater.* **2007**, *105*, 298–304. [CrossRef]
42. Shaban, M.; AbuKhadra, M.R.; Nasief, F.M.; Abd El-Salam, H.M. Removal of Ammonia from Aqueous Solutions, Ground Water, and Wastewater Using Mechanically Activated Clinoptilolite and Synthetic Zeolite-A: Kinetic and Equilibrium Studies. *Water Air Soil Pollut.* **2017**, *228*, 450. [CrossRef]
43. Shoumkova, A. Zeolites for Water and Wastewater Treatment: An Overview. In *2011 Research Bulletin of Australian Institute of High Energetic Materials*; Australian Institute of High Energetic Materials: Sippy Downs, QLD, Australia, 2012.
44. Fu, H.; Li, Y.; Yu, Z.; Shen, J.; Li, J.; Zhang, M.; Ding, T.; Xu, L.; Lee, S.S. Ammonium Removal Using a Calcined Natural Zeolite Modified with Sodium Nitrate. *J. Hazard. Mater.* **2020**, *393*, 122481. [CrossRef] [PubMed]
45. Shi, K.; Wang, Z.; Luo, J.; Qian, G.; Luo, Y.; Li, M.; Yao, H. Construction of Novel NH2-Al-SBA-15 Based Mesoporous Molecular Sieve and Application in the Adsorption of Methylene Blue. *J. Porous Mater.* **2024**, *31*, 2017–2029. [CrossRef]
46. Li, X.; Li, Y.; Li, Y.; Zhang, M.; Zhu, J. Synthesis of Lignin-Derived Hierarchical Porous Carbon via Hydrothermal–Phosphoric Acid Synergistic Activation for Enhanced Adsorption of Tetracycline. *Molecules* **2026**, *31*, 447. [CrossRef] [PubMed]

47. Greathouse, J.A.; Paul, M.J.; Xu, G.; Powell, M.D. Molecular Dynamics Simulation of Pore-Size Effects on Gas Adsorption Kinetics in Zeolites. *Clays Clay Miner.* **2023**, *71*, 54–73. [CrossRef]
48. Cui, Y.; Wang, Y.; Li, B.; Huang, J.; Bo, L.; Liu, H.; Mathe, M.K.; Samadiy, M.; Guo, S.; Shen, H.; et al. Integrating Overall Water Splitting with Advanced Oxidation for Wastewater Treatment Using a Bifunctional Medium-Entropy Amorphous Alloy. *Nano-Micro Lett.* **2026**, *18*, 333. [CrossRef] [PubMed]
49. Marković, D.D.; Lekić, B.M.; Rajaković-Ognjanović, V.N.; Onjia, A.E.; Rajaković, L.V. A New Approach in Regression Analysis for Modeling Adsorption Isotherms. *Sci. World J.* **2014**, *2014*, 930879. [CrossRef] [PubMed]
50. Maksin, D.; Kljajevic, S.; Djolic, M.; Markovic, J.; Ekmescic, B.; Onjia, A.; Nastasovic, A. Kinetic Modeling of Heavy Metal Sorption by Vinyl Pyridine Based Copolymer. *Hem. Ind.* **2012**, *66*, 795–804. [CrossRef]
51. Chen, S.; Deng, J.; Wang, L.; Ma, X.; Xu, M.; Xu, D.; Wang, H.; Shi, W. Comparison of Vacuum Ultraviolet-Based Oxidation as Ultrafiltration Pretreatment in Real Water: Performance, Risk Assessment, and Mechanistic Insights. *Water Res.* **2026**, *298*, 125801. [CrossRef] [PubMed]
52. Huang, H.; Xiao, X.; Yan, B.; Yang, L. Ammonium Removal from Aqueous Solutions by Using Natural Chinese (Chende) Zeolite as Adsorbent. *J. Hazard. Mater.* **2010**, *175*, 247–252. [CrossRef] [PubMed]
53. Vocciante, M.; De Folly D'Auris, A.; Finocchi, A.; Tagliabue, M.; Bellettato, M.; Ferrucci, A.; Reverberi, A.P.; Ferro, S. Adsorption of Ammonium on Clinoptilolite in Presence of Competing Cations: Investigation on Groundwater Remediation. *J. Clean. Prod.* **2018**, *198*, 480–487. [CrossRef]
54. Huang, L.; Jiao, X.; Lin, J.; Hao, J.; Tan, L.; Zeng, D.; Wang, S.; Lu, Y.; Shen, X.; Zhang, Z.; et al. EGDE-Induced Crosslinking of PEI@D500 Adsorbents for Direct Air Capture: Enhanced Hydrothermal and Oxidative Stability. *Chem. Eng. J.* **2026**, *537*, 176243. [CrossRef]
55. Wang, D.; Hu, W.; Zheng, Y.; Xia, Z.; Cheng, H.; Lu, X.; He, Z.; Giannakis, S.; Song, S.; Ma, J. Mechanistic Insights into Hexamethylphosphoramide Degradation and Phosphorus Recovery via mZVI/$O_3$: Beyond Conventional Oxidation through Iron-Phosphorus Speciation. *Chem. Eng. J.* **2026**, *538*, 176658. [CrossRef]
56. Tian, G.; Chen, H.; Jiang, R.; Zhang, C.; Lu, X.; Wang, X.; Wei, F. A Dual-Engine Artificial Intelligence Framework Accelerates Sustainable Aviation Fuel Component Synthesis. *J. Am. Chem. Soc.* **2026**, *148*, 9879–9891. [CrossRef] [PubMed]
57. Tian, G.; Wang, Z.; Zhang, C.; Wei, F. Nano Bifunctional Catalysts as Miniaturized Chemical Processes for $CO_x$-to-Aromatics Conversion. *Acc. Chem. Res.* **2026**, *59*, 646–658. [CrossRef] [PubMed]


**Disclaimer/Publisher's Note:** The statements, opinions and data contained in all publications are solely those of the individual author(s) and contributor(s) and not of MDPI and/or the editor(s). MDPI and/or the editor(s) disclaim responsibility for any injury to people or property resulting from any ideas, methods, instructions or products referred to in the content.